Wind and Structures, Vol. 8, No. 2 (2005) 107-120 107
DOI: http://dx.doi.org/10.12989/was.2005.8.2.107

Steady wind force coefficients of inclined stay cables with water rivulet and their application to aerodynamics

Masaru Matsumoto†, Tomomi Yagi‡, Seiichiro Sakai‡†,
Jun Ohya‡† and Takao Okada‡†

Department of Civil and Earth Resources Engineering, Kyoto University, Yoshida Honmachi, Sakyo-ku, Kyoto 606-8501, Japan
Advanced Research Institute of Fluids Science and Engineering, Int'tech Center, Kyoto University, Katsura Campus, Nishikyo-ku, Kyoto 615-8510, Japan

(Received January 9, 2004, Accepted August 5, 2004)

Abstract. The quasi-steady approaches to simulate the wind induced vibrations of inclined cables, especially on the rain-wind induced vibration, have been tried by many researchers. However, the steady wind force coefficients used in those methods include only the effects of water rivulet, but not the axial flow effects. The problem is the direct application of the conventional techniques to the inclined cable aerodynamics. Therefore, in this study, the method to implement the axial flow effects in the quasi-steady theory is considered and its applicability to the inclined cable aerodynamics is investigated. Then, it becomes clear that the perforated splitter plate in the wake of non-yawed circular cylinder can include the effects of axial flow in the steady wind force coefficients for inclined cables to a certain extent. Using the lateral force coefficients measured in this study, the quasi-steady theory may explain the wind induced instabilities of the inclined cables only in the relatively high reduced wind velocity region. When the Scruton number is less than around 40, the high speed vortex-induced vibration occurs around the onset wind velocity region of the galloping, and then, the quasi-steady approach cannot be applied for estimating the response of wind-induced vibration of inclined cable.

Keywords: inclined stay cable; rain-wind induced vibration; galloping; high-speed vortex-induced vibration; steady wind force coefficients; quasi-steady theory.

1. Introduction

The wind-induced vibrations of inclined stay cables, especially on the rain-wind induced vibration, have been investigated using various methods, for example, wind tunnel tests, field observations, numerical approaches and so on. The main factors for generating rain-wind induced vibration must be considered as the upper water rivulet due to the rainfall and the axial flow due to the cable inclination (Matsumoto, *et al*. 1992). Also, from the field observation results of the real stay cables, this kind of vibration usually observed at the limited reduced wind velocity region around $V/fD=20$, 40, and so on, where V is a wind velocity, f is a frequency of vibration and D is a

† Professor, Corresponding Author, E-mail: matsu@brdgeng.gee.kyoto-u.ac.jp
‡ Research Associate
‡† Former Graduate Student

diameter of cable (Matsumoto, *et al*. 1997). To explain the rain-wind induced vibration, some approaches have been tried, for example, interpreting the vibration as high speed vortex-induced vibration, which is related to complex three dimensional and unsteady properties of vortices around the cable (Matsumoto 1998), or simulating the response by the quasi-steady theory for a circular cylinder with water rivulet, which kinds of research works have been reported in many papers (e.g. Yamaguchi 1990, Gu and Lu 2001, Xu and Wang 2003) recently. The latter approach is based on the traditional quasi-steady theory for the galloping, and to realize the velocity restricted phenomena the effects of moving rivulet are introduced in their equations of motion. It is needless to say that these models for the rain-wind induced vibration cannot simulate the phenomena concerned with the vortices. Furthermore, the effects of axial flow, which appears in the wake of cable due to the cable inclination, are not included in these models. Using a rigid circular cylinder supported horizontally with certain yaw angle by springs in the wind tunnel, the galloping oscillation can easily occur without any rivulets on the surface. This vibration is due to the axial flow and its instability is never included in their models. Because the steady wind force coefficients used in their studies were measured using a circular cylinder with artificial water rivulet mounted in the wind tunnel without any inclination or yawing, and furthermore, even conducting the experiments under inclined or yawed situation, the effects of axial flow never appears on these coefficients, which details will be explained later. Therefore, the aim of this study is to consider and develop the method to implement the axial flow effects in the quasi-steady theory and to investigate its applicability to the simulation of the inclined cable aerodynamics.

The factors to induce the negative value of the slope of lateral force coefficients $dC_F/d\alpha$, which is defined later, in the inclined stay cables must be the upper water rivulet and the axial flow. The conventional way to measure the steady wind forces for the cable models can only include the effect of water rivulet installing the artificial one on its surface. However, the effect of axial flow has been never considered as mentioned before. The effects of axial flow on the cable aerodynamics must be the similar effects to the splitter plate in the wake of circular cylinder, which forms the inner circulatory flow in the wake of cylinder. Then, to simulate the axial flow effects on the inclined cables, the special splitter plate was proposed and their steady wind forces were measured. Also, using those steady wind forces, the applicability of quasi-steady theory will be discussed.

The idea of moving water rivulet, which can be seen in the papers (e.g. Yamaguchi 1990, Gu and Lu 2001, Xu and Wang 2003), is not incorporated into this study. The fact of the rivulet movement induced by the cable motion or the wind turbulence must be true. However, it is not easy to believe that the water rivulet motion can coupled with the cable motion through a long stay-cable. Therefore, in this study, it is considered that the effects of water rivulet on the cable aerodynamics must be defined by the average position of water rivulet.

2. Problems on conventional quasi-steady approach

First of all, it is needless to say that an application of the quasi-steady approach to the rain-wind induced vibration means an analysis of its instability as a galloping type. As mentioned above, the conventional quasi-steady approach has not included the effects of axial flow, even using the steady wind force coefficients of circular cylinder measured under inclined or yawed situations. For example, a yawed circular cylinder without any rivulet can easily vibrate in the wind tunnel. However, this galloping phenomenon due to the axial flow cannot be explained by the conventional quasi-

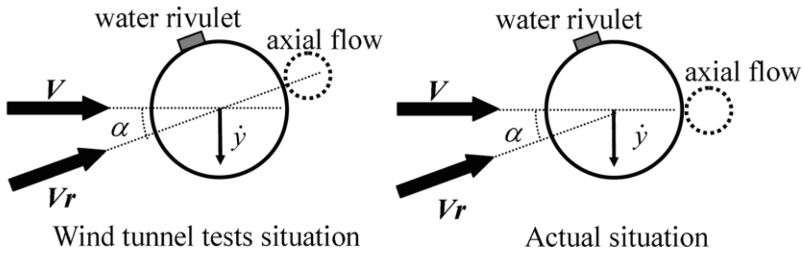

Fig. 1 Position of axial flow

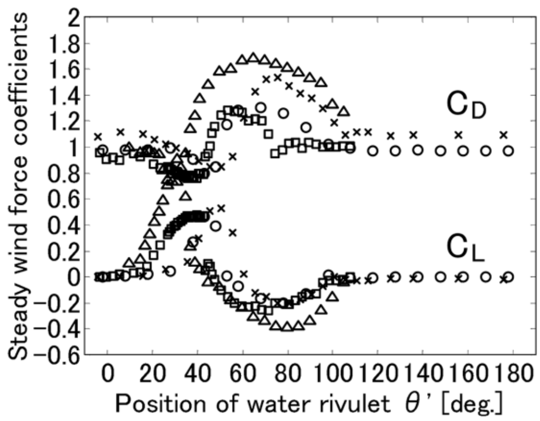

○: D=50mm, rectangular rivulet (thickness:1.6mm and width:3.6mm)

×: D=50mm, rectangular rivulet (thickness:1.2mm and width:7.5mm)

△: Yamaguchi, d/D=0.1 circular rivulet (d: diameter of circular rivulet)

□: Gu, D=120mm, half ellipse rivulet (long axis 14.5mm, short axis 10.0mm)

Fig. 2 Effects of shape of rivulet on steady wind force coefficients

steady approach. To explain this, the positions of the axial flow are shown in Fig. 1. In the situation for measuring the steady wind force coefficients of yawed cylinder, the axial flow occurs in the wake center of the relative wind, which corresponds to the wind in the wind tunnel. However, in the actual case, the axial flow must be situated in the wake center of the actual wind. Therefore, in the wind tunnel situation, the position of axial flow is fixed against the relative wind. Then, the effects of axial flow cannot appear on the slope of lateral force coefficients $dC_F/d\alpha$.

This axial flow has a similar role to the splitter plate in the wake of circular cylinder, which forms the inner circulatory flow in the wake of cylinder. To realize the effects of the axial flow on the cable model, a perforated splitter plate in the wake of non-yawed cable model was tried to use in this study. The position of this plate against the approaching flow can be changed.

Generally, for the simulating the effects of water rivulet, the artificial rivulet are installed on the surface of cable model. In Fig. 2, the wind force coefficients are compared against various shapes of rivulet, which are rectangular rivulets from authors, a circular one from Yamaguchi (1990) and a half ellipse one from Gu and Lu (2001). In this figure, the position of rivulet is determined by the angle θ from the stagnation point to its front edge, instead of the center of the rivulet usually defined as θ. Then, it seems that the wind force coefficients are rather sensitive to the shapes of rivulet. Therefore, it must be noted that the results of the quasi-steady approach rather depend on the shape of artificial water rivulet.

3. Wind tunnel tests

The wind tunnel used in this study is a room-circuit Eiffel type located in Kyoto University. The working section of the wind tunnel is 1.8 m height and 1.0 m width, and the maximum wind velocity is 30 m/s. A rigid cable model used in the steady wind force measurements was an aluminum circular cylinder with diameter $D = 50$ mm, length $L = 1060$ mm. This model was mounted horizontally without any yawing angle in the wind tunnel. To realize the upper water rivulet on the cable surface, an artificial rectangular rivulet (thickness: 1.6 mm, width: 3.6 mm) was installed at the various angles $\theta = 0^o - 180^o$ from the stagnation point of cable model, as shown in Fig. 3. Also, to simulate the axial flow effects, a splitter plate with the length 4*D* and 30% perforation as shown in Fig. 4, was installed at the angle $\varepsilon = 176^o - 184^o$ from the stagnation point, as shown in Fig. 3. The distance between the cylinder and the plate is 0.1*D*. The lift (*L*) and drag (*D*) forces of the stationary cable model were measured using load-cells at the both ends of model, which are corresponds to the forces against the relative wind velocity V_r, as shown in Fig. 5. In this study, the lateral force (*F*) against approaching wind velocity *V* is defined as shown in Fig. 5, and this can be determined by *L*, *D* and the relative angle of attack α.

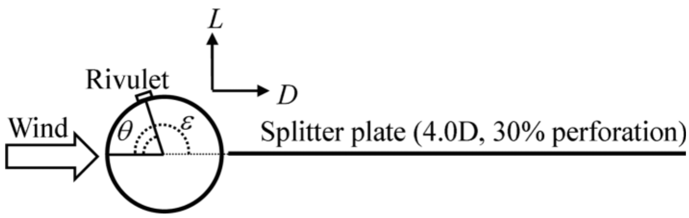

Fig. 3 Position of rivulet and splitter plate in the wind tunnel

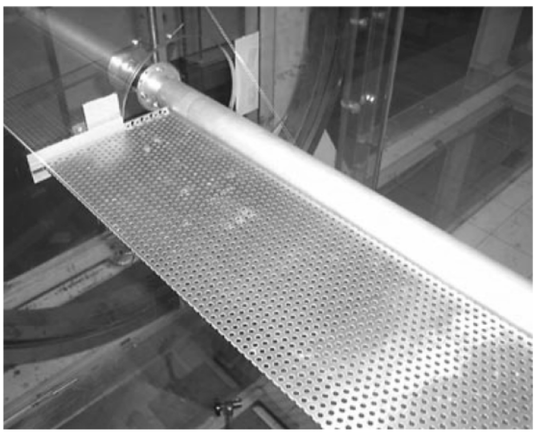

Fig. 4 Perforated splitter plate (PSP)

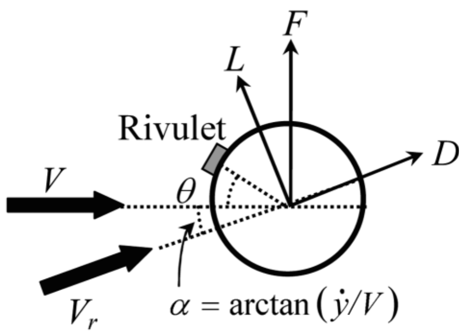

Fig. 5 Relative angle of attack α and lateral force *F*

For the verification, some static and dynamic tests using rigid yawed circular cylinder with the yawing angle $\beta = 45^{\circ}$ were also conducted. This model is made of aluminum pipe and covered by a thin wooden plate, and its diameter is $D = 54$ mm and the length is $L = 1500$ mm. In these experiments, the cylinder bored through the wall of wind tunnel with circular holes (110 mm diameter) at the both up-stream and down-stream sides. All of the wind tunnel tests were conducted at the Reynolds number in the sub-critical range in this study.

4. Verification of effects of perforated splitter plate as axial flow

The axial flow in the wake of inclined cable must have similar effects as a splitter plate in the wake of cylinder. This flow or plate can form inner circulatory flow in the wake and induce the galloping instability. However, a solid splitter plate intensively reduces the Karman vortex sheddings. In general, the Karman vortices exist in the wake of inclined cables, and actually, Karman vortex related phenomena, such as the conventional Karman vortex vibration and the high speed vortex induced vibration (Matsumoto 1998) can be seen in the inclined cables. Therefore, a flow field around a non-yawed circular cylinder with the solid splitter plate may be different form one around the inclined cable. Then, in this study, a perforated splitter plate is introduced to reduce destruction of the Karman vortices in the wake of non-yawed circular cylinder.

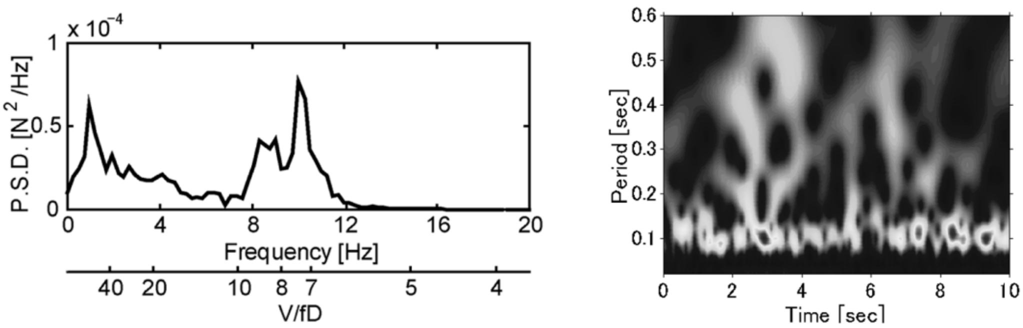

Fig. 6 PSD and wavelet analysis of fluctuating lift force on yawed stationary cable model ($\beta = 45^{\circ}$, in smooth flow, $V = 4.0$ m/s)

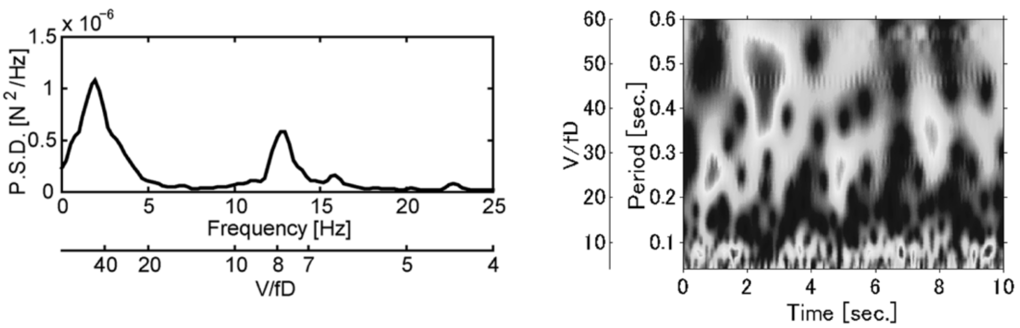

Fig. 7 PSD and wavelet analysis of fluctuating lift force on non-yawed stationary cable model with perforated splitter plate (with PSP, $\beta = 0^{\circ}$, in smooth flow, $V = 5.0$ m/s)

To compare the flow fields in the wake of the yawed cable model and non-yawed circular cylinder with the perforated splitter plate, the unsteady lift force of both models were measured. The diagrams of the power spectrum density (abbreviated as PSD) and the wavelet analysis of the fluctuating lift force on stationary yawed circular cylinder ($\beta = 45^{o}$) are shown in Fig. 6. In the PSD diagram, the Karman vortex components can be seen around reduced wind velocity around 7, which corresponds to the Strouhal number around 0.14 and this value is rather lower than 0.2 of the non-yawed cylinder case. Furthermore, there are very low frequency components, which correspond to the high speed vortex induced vibration, and these components are rather unsteady as shown in the result of the wavelet analysis. These low frequency components must be related to the unsteady and three dimensional properties of the Karman vortex. Therefore, even using the splitter plate, the intensive reduction of the Karman vortex should be avoided. This means that the fluid interaction between two separated shear layers around the cylinder must be necessary. Then, the length of the splitter plate and the perforation ratio were tried to vary to find the similar wake condition as the yawed circular cylinder ($\beta = 45^{o}$). In consequence, the non-yawed cylinder with the perforated splitter plate at $\varepsilon = 180^{o}$, which length is 4.0*D* and opening ratio is 30%, has rather similar aerodynamic properties as the yawed cylinder ($\beta = 45^{o}$), as shown in Fig. 7. Therefore, in this study, it is assumed that the wake conditions between the yawed cylinder and the non-yawed cylinder with this plate are similar. Then, the 30% perforated splitter plate (4.0*D*) is used to simulate the axial flow effects, and this plate will be abbreviated as PSP in this paper.

5. Steady wind force coefficients

The steady drag and lift force coefficients C_D and C_L can be defined as follows:

$$C_D = \frac{Drag}{\frac{1}{2}\rho V_w^2 A} \tag{1}$$

$$C_L = \frac{Lift}{\frac{1}{2}\rho V_w^2 A} \tag{2}$$

where *Drag* and *Lift* denote the steady drag and lift forces (N/m) and ρ, V_w, A are the air density (kg/m^3), the wind velocity in the wind tunnel (m/s), the projected area (m^2/m), respectively. This wind velocity V_w corresponds to the relative wind velocity V_r in Fig. 5.

First of all, the steady lift and drag force coefficients C_L and C_D of the circular cylinder with the artificial water rivulet are compared among the cable models, which are 1) non-yawed cylinder, 2) yawed cylinder ($\beta = 45^{o}$) and 3) non-yawed cylinder with PSP at $\varepsilon = 180^{o}$, as shown in Fig. 8. The characteristics of C_L diagrams between the non-yawed model 1), 2) and the yawed model 3) are qualitatively similar, except about 5^{o} differences on the position of rivulet for the maximum C_L. In C_D diagrams, all of the plots have rather similar characteristics, but their values are quite different each other. However, using the PSP for the non-yawed model, its C_D properties become closer to the yawed model ones.

Varying the PSP from $\varepsilon = 176^{o}$ to 184^{o} and the rivulet from $\theta = 0^{o}$ to 180^{o} on the non-yawed cable model, the lift force coefficient C_L and the drag force coefficient C_D are shown in Fig. 9. Around the position of water rivulet $\theta = 30^{o}-60^{o}$, C_L and C_D values dramatically changes against θ. On the

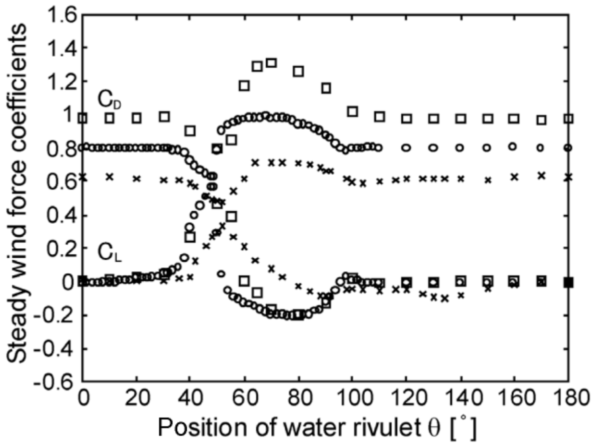

Fig. 8 Steady wind force coefficients of various cable models with water rivulet (V = 8.0 m/s, in smooth flow, ○: β = 0°, with PSP, □: β = 0°, without PSP, x : β = 45°)

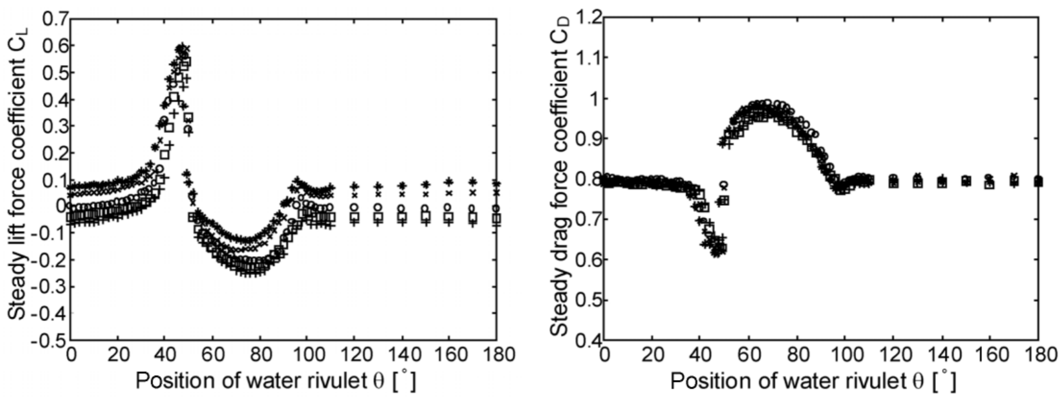

Fig. 9 Steady lift and drag force coefficients of non-yawed cable with PSP and water rivulet (β = 0°, V = 8.0 m/s, in smooth flow, * : ε = 176°, x : ε = 178°, ○: ε = 180°, □: ε = 182°, + : ε = 184°)

other hand, the variations of C_L and C_D against the position of PSP are quite similar through the all range of θ. Then, it seems that the effects of water rivulet are dominant around $\theta = 30^\circ - 60^\circ$ comparing with the effects of PSP.

These coefficients can be used to determine the lateral force coefficient $C_F(\theta, \alpha)$, where θ is the position of water rivulet and α denotes the relative angle of attack between -4° to +4°, see Fig. 5. Then, the lateral force coefficient C_F can be defined as the following equation using C_L and C_D.

$$C_F(\theta, \alpha) = (C_D(\theta + \alpha)\sin\alpha + C_L(\theta + \alpha)\cos\alpha)(1/\cos^2\alpha) \tag{3}$$

Therefore, for the each position of water rivulet θ, the lateral force coefficient C_F can be determined at the relative angle of attack α = -4°, -2°, 0°, +2°, +4°. As an example, C_F of θ = 72° is shown in Fig. 10. In this figure, dashed lines denote the lateral force coefficient against the angle of attack with the fixed PSP, which is the similar condition as the conventional wind tunnel situation as

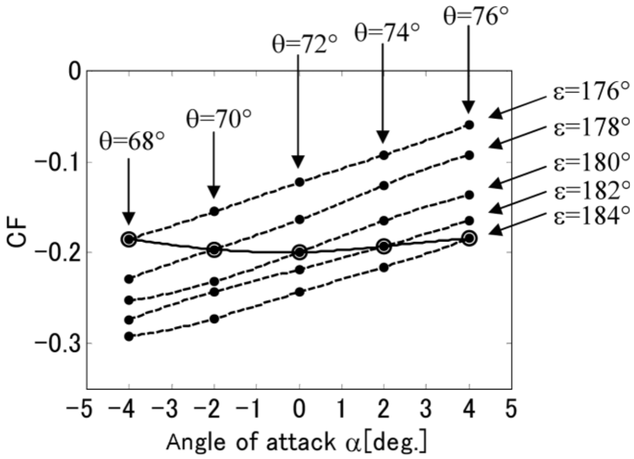

Fig. 10 Lateral force coefficient C_F against angle of attack at the rivulet position $\theta = 72^o$ ($V = 8.0$ m/s, in smooth flow, dashed line : $\beta = 0^o$, with fixed PSP, solid line : $\beta = 0^o$, with effective PSP)

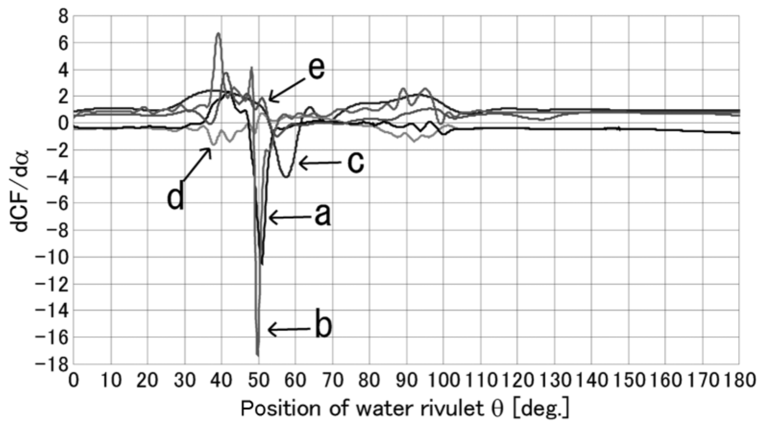

Fig. 11 Slope of lateral force coefficient $dC_F/d\alpha$ against position of water rivulet ($V = 8.0$ m/s, in smooth flow, (a) : $\beta = 0^o$, with PSP, (b) : $\beta = 0^o$, with fixed PSP ($\varepsilon = 180^o$), (c) : $\beta = 0^o$, without PSP, (d) : $\beta = 0^o$, with PSP, fixed water rivulet, (e) : $\beta = 45^o$, without PSP)

shown in Fig. 1, and their slopes are positive. On the other hand, the solid line shows the coefficients, which include the effects of axial flow simulated by the PSP, and then the slope changes to negative values in the negative region of α. Then, the slopes of lateral force coefficient $dC_F/d\alpha$ around $\alpha = 0^o$ are evaluated and plotted at the position of water rivulet $\theta = 72^o$ in Fig. 11. Plotting the data of $dC_F/d\alpha$ around $\alpha = 0^o$ for each θ, finally the curve (a) in Fig. 11 is completed. To compare the effects of water rivulet, axial flow and so on, the five ways for calculating $dC_F/d\alpha$ are tried as follows:

(a) Non-yawed circular cylinder with the water rivulet and the PSP, where $\beta = 0^o$.
(This is the basic case, which includes both water rivulet and splitter plate effects, and this situation is rather similar to actual situation shown in Fig. 1)

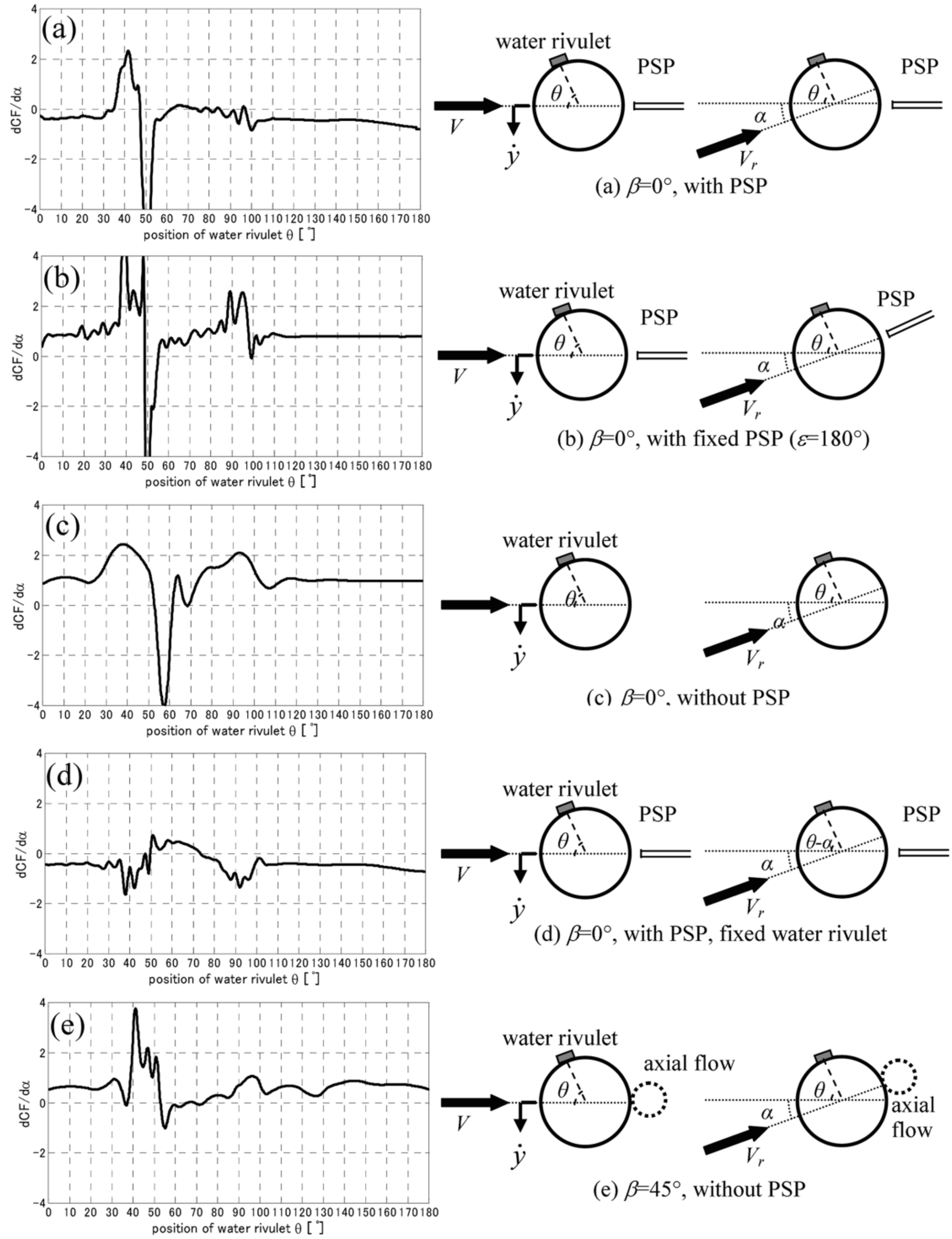

Fig. 12 Detail diagrams for $dC_F/d\alpha$ against position of water rivulet with illustrations (V = 8.0 m/s, in smooth flow (a) β = 0°, with PSP, (b) β = 0°, with fixed PSP (ε = 180°), (c) β = 0°, without PSP, (d) β = 0°, with PSP, fixed water rivulet, and (e) β = 45°, without PSP)

(b) Non-yawed circular cylinder with the water rivulet and the FIXED PSP at the wake center of relative wind, where $\varepsilon = 180^o$, $\beta = 0^o$.
(Therefore, there are no effects of splitter plate on $dC_F/d\alpha$, but on the original data of C_D and C_L. This means the splitter plate synchronized with the body motion to keep the same position as in the wake center against the relative wind)
(c) Non-yawed circular cylinder with the water rivulet and WITHOUT the PSP, where $\beta = 0^o$.
(There are totally no effects of the splitter plate. However, the data are available with rough intervals of θ)
(d) Non-yawed circular cylinder with the PSP and the FIXED water rivulet, where $\beta = 0^o$.
(Therefore, there are no effects of water rivulet on $dC_F/d\alpha$, but on the original data of C_D and C_L. This means the water rivulet synchronized with the body motion to keep the same position of θ against the relative wind)
(e) Yawed circular cylinder with the water rivulet and without the PSP, where $\beta = 45^o$.
(As mentioned before, in this case, there are no effects of axial flow on $dC_F/d\alpha$, which is shown in Fig. 1 as the wind tunnel tests situation)

Fig. 11 shows that these curves are different each other, especially on the negative region of $dC_F/d\alpha$ against the position of water rivulet. Therefore, the effects of the PSP, that is the effect of axial flow, seem to have important roles on inclined cable aerodynamics. To show the detail of Fig. 11, $dC_F/d\alpha$ of the each case are plotted separately with the illustrations of the wind tunnel tests situations in Fig. 12. In the case (a), which includes the both effects of water rivulet and PSP, $dC_F/d\alpha$ has explicit negative values at the rivulet position around $\theta = 0^o-30^o$, 45^o-65^o, and 100^o-180^o. Also, in the case (d), which includes only the PSP effects, $dC_F/d\alpha$ is negative around $\theta = 0^o-50^o$ and 75^o-180^o. On the other hand, in the cases (b), (c), (e), which consider the water rivulet effects only, the negative values appear only around the water rivulet poison around $\theta = 50^o-65^o$. Therefore, using the PSP, the galloping instability induced by the axial flow becomes possible to include in the slope of lateral force coefficients $dC_F/d\alpha$ to a certain extent. Then, it can be concluded that the instability at the rivulet position around $\theta = 0^o-30^o$, 100^o-180^o is induced by the axial flow, and in the unstable region around $\theta = 50^o-65^o$, the effects of water rivulet are dominant.

6. Application of quasi-steady theory

For the non-linear analysis basing on the quasi-steady theory, the lateral force coefficient C_F is expressed into the polynomial form up to seventh term associated to relative angle of attack α in terms of the cross-flow response velocity $\dot{y}$ as follows (Parkinson and Brooks 1961) :

$$C_F = A_1 + A_2\alpha + A_3\alpha^2 + A_4\alpha^3 + A_5\alpha^4 + A_6\alpha^5 + A_7\alpha^6 + A_8\alpha^7 \quad (4)$$

$$\alpha = \arctan(\dot{y}/V) = (\dot{y}/V) - (1/3)(\dot{y}/V)^3 + (1/5)(\dot{y}/V)^5 - (1/7)(\dot{y}/V)^7 \quad (5)$$

Using the Krylov-Bogoliubov approximate method, the limit cycle amplitudes at each reduced velocity are obtained as well as the critical galloping reduced velocity, which theoretically coincides to the result from Den Hartog's criteria. For the situation (a), in which the axial flow is simulated by the PSP, the lateral force coefficients $C_F(\theta, \alpha)$ can be only defined at the range of $\pm 4^o$ relative

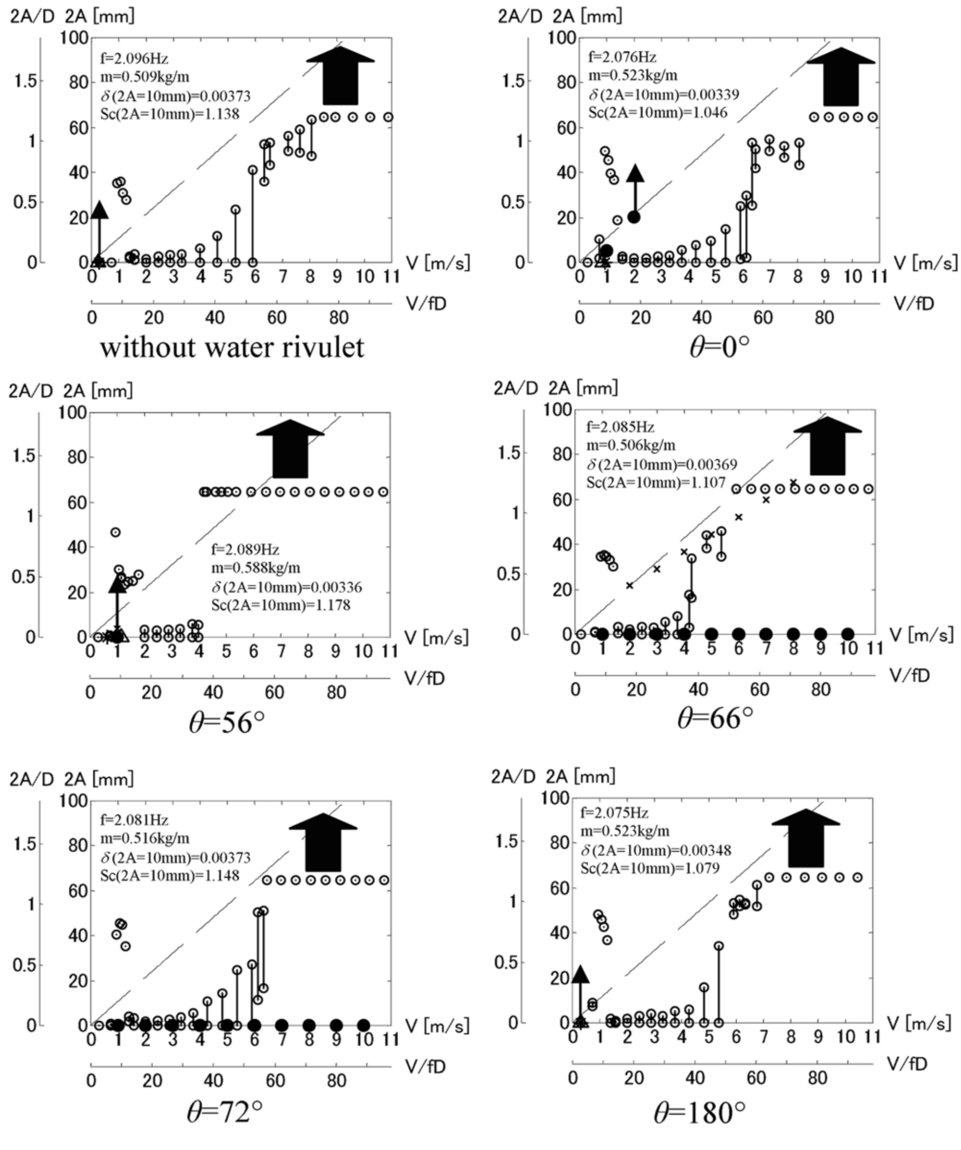

Fig. 13 V-A diagrams of yawed cable model $\beta = 45^{\mathrm{o}}$ with rivulet and results of quasi-steady analyses using C_F of case (c) (in smooth flow, o:wind tunnel tests, ●: quasi-steady analyses, x: limit cycle, *: critical wind velocity of Den Hartog's criteria, Δ: critical wind velocity of Parkinson's method)

angle of attack. Therefore, the amplitudes calculated from this theory are limited at the range of ±4$^{\mathrm{o}}$ relative angle of attack, if C_F of the case (a) is used. The boundary of the available amplitude is indicated by a dashed line in the velocity-amplitude (V-A) diagrams. In another words, the smaller amplitudes below the dashed lines can be compared with the experimental results. In Fig. 13, the V-A diagrams of the yawed cable ($\beta = 45^{\mathrm{o}}$) under the condition of small Scruton number, such as approximately 1, in smooth flow obtained from the wind tunnel tests and the non-linear analyses using C_F of the case (a) are compared for the various rivulet positions, which are $\theta = 0^{\mathrm{o}}$, 56^{o}, 66^{o},

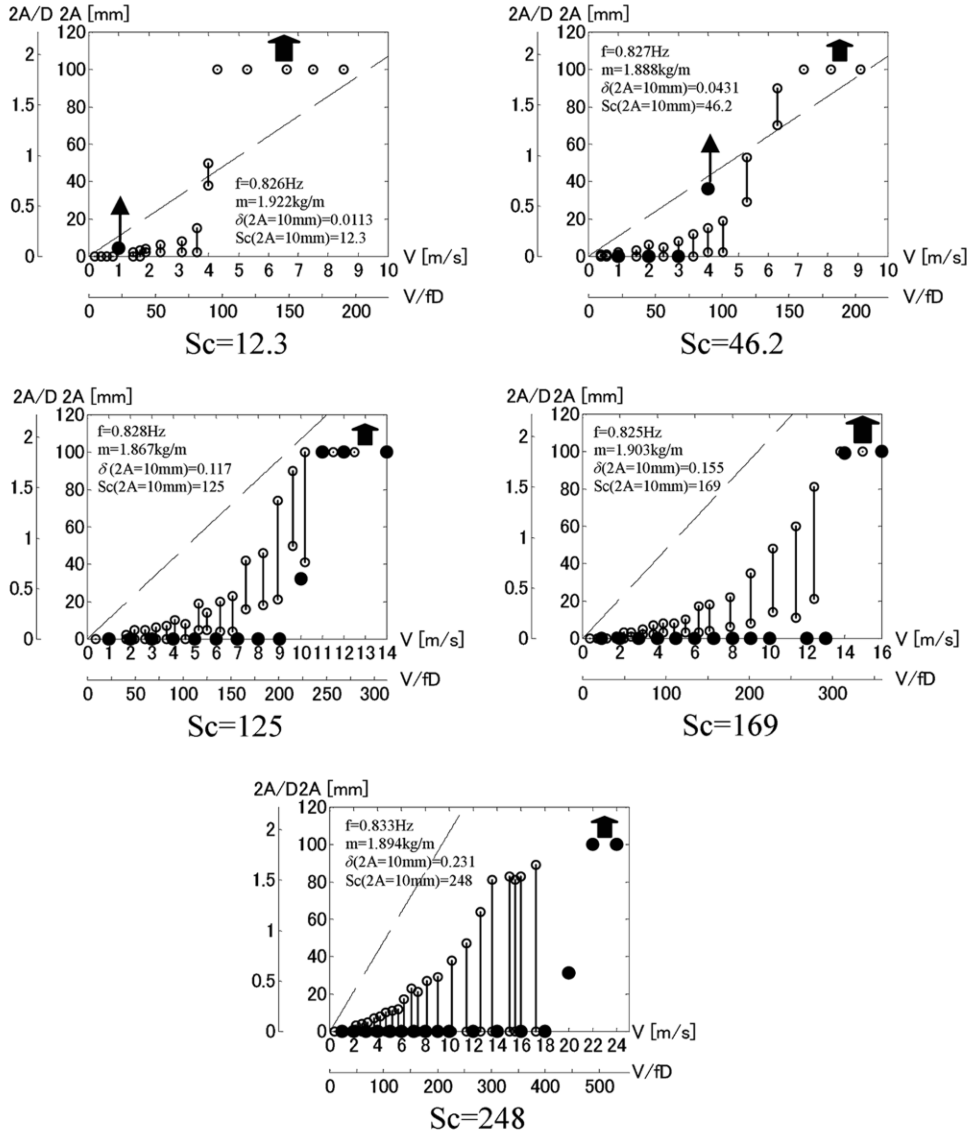

Fig. 14 V-A diagrams of yawed cable model $\beta = 45^{o}$ without rivulet and results of quasi-steady analyses using C_F of case (a) in various Sc numbers (in smooth flow, ○ : wind tunnel tests, ●: quasi-steady analyses)

72^{o}, 180^{o} and without rivulet case. The Scruton number can be defined as $Sc = 2m\delta/\rho D^2$, where m, δ, ρ, D denote the mass per length, the logarithmic decrement, the air density and the diameter of cylinder, respectively. Experimentally, the galloping appears at approximately reduced wind velocity $V/fD = 40$ for these all cases. However, from the non-linear analysis, the galloping appears at much lower reduced velocity. Exceptionally at the case of $\theta = 66^{o}$ and 72^{o}, the galloping instability has the amplitude dependence or stable characteristics. The galloping vibration of $\theta = 66^{o}$ and 72^{o} in the wind tunnel seems to be triggered by the certain vortex with longer period than Karman vortex,

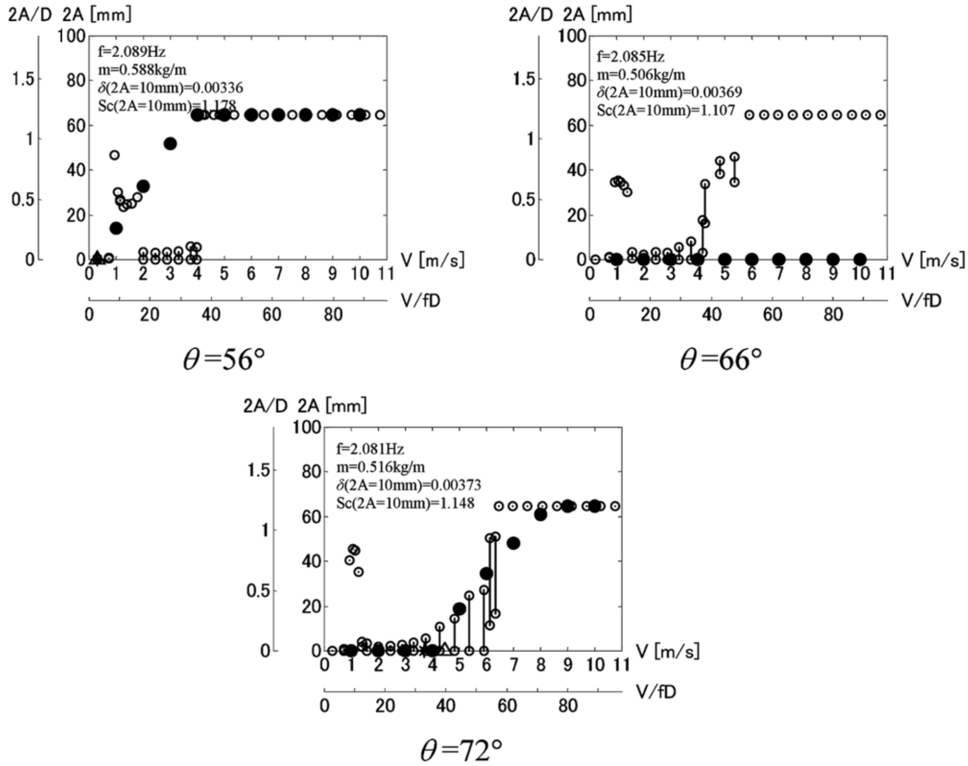

Fig. 15 V-A diagrams of yawed cable model $\beta = 45^{\circ}$ with rivulet and quasi-steady analyses using C_F of case (e) (in smooth flow, ○: wind tunnel test, ●: quasi-steady analysis, x: limit cycle, *: critical wind velocity of Den Hartog's criteria, Δ: critical wind velocity of Parkinson's method)

which is the high speed vortex-induced vibration.

On the other hand, for large Scruton number, the analyzed response of the yawed cable without a rivulet in smooth flow, using C_F of the case (a), tends to coincide with the experimental results as shown in Fig. 14. Then, it became clear that the response of galloping cannot be estimated by this quasi-steady theory, when the Scruton number *Sc* is less than 40. On the other hand, there are better agreements in the onset wind velocity and the responses when the *Sc* is larger than 40.

These results seem to be rather similar to the case of non-yawed rectangular cylinder. In that case, the Karman vortex-induced vibration occurs in the near wind velocity region of the onset velocity of the galloping. Or, it can be said that the galloping occurs in connection with the Karman vortex-induced vibration. Therefore, the onset wind velocity of galloping is strongly related to the Karman vortex, and of course, the quasi-steady theory cannot explain the vortex related phenomena. In case of the inclined cable model, the high speed vortex-induced vibration occurs around the onset wind velocity region of the galloping, instead of the Karman vortex-induced vibaration. However, the quasi-steady theory can apply to the rectangular cylinder and even to the inclined cable model in the high reduced wind velocity region.

The analytical responses of yawed cable in smooth flow with the upper rivulet at $\theta = 56^{\circ}$, 66° and 72°, using C_F of the case (e), are compared with the experimental ones in Fig. 15. This C_F of the case (e) was measured in the wind tunnel situation of Fig. 1, which means that the real axial flow exists in the wake, but there is any effect against the relative wind. In the response of the case of $\theta = 72^o$, the analytical V-A diagram shows a fairly well agreement with the experimental one, but it can be said to be accidental. Because the other cases show the significant differences between the experiments and the analyses, including the cases at $\theta = 0^o$ and 180^o, where the galloping does not occur at all in the analyses.

From these results, there are still subjects in application of the quasi-steady theory to evaluate the inclined cable aerodynamics, in particular, the rain-wind induced vibration. Moreover, the wind-induced vibration of the inclined/yawed cable without/with an upper rivulet should be related to the high-speed vortex excitation.

7. Conclusions

In this paper, the method to implement the axial flow effects of the inclined cables in the quasi-steady theory is investigated and its applicability to the inclined cable aerodynamics is also considered. Then, it becomes clear that the perforated splitter plate (PSP) in the wake of non-yawed circular cylinder can include the effects of axial flow in the steady wind force coefficients to a certain extent. Considering the slope of lateral force coefficients, there are two factors to induce the galloping instabilities of the inclined cables, which are the water rivulet and the axial flow simulated by PSP. Using the lateral force coefficients measured in this study, the quasi-steady theory may explain the wind induced instabilities of the inclined cables only in the relatively high reduced wind velocity region. When the Scruton number is less than around 40, the high speed vortex-induced vibration occurs around the onset wind velocity region of the galloping, and then, the quasi-steady approach cannot be applied for estimating the response of the inclined cable.

Acknowledgements

This work was supported in part by Grant-in-Aid for Scientific Research (A) No. 12305030 from Japan Society for the Promotion of Science. Finally, the authors highly appreciate Mr. Takahiro Oishi, Kyoto University for his help on a series of wind tunnel tests.

References

Gu, M. and Lu, Q. (2001), “Theoretical analysis of wind-rain induced vibration of cables cable-stayed bridges”, *Proceedings of 5th Asia-Pacific Conference on Wind Engineering*, Kyoto, Japan, 125-128.

Matsumoto, M., Shiraishi, N. and Shirato, H. (1992), “Rain-wind induced vibration of cables of cable-stayed bridges”, *J. Wind Eng. Ind. Aerodyn.*, **41-44**, 2011-2022.

Matsumoto, M., Shigemura, Y., Daito, Y. and Kanamura, T. (1997), “High speed vortex shedding vibration of inclined cables”, *Proceedings of International Seminar on Cable Dynamics*, Tokyo, Japan, 27-35.

Matsumoto, M. (1998), “Observed behavior of prototype cable vibration and its generation mechanism”, In Larsen, Larose & Liversey (Eds.), *Bridge Aerodynamics*, Balkema, Rotterdam, 189-211.

Parkinson, G.V. and Brooks, N.P.H. (1961), “On the aeroelastic instability of bluff cylinders”, *J. Appl. Mech., Transactions*, ASME, **28**, 252-258.

Xu, Y.L. and Wang, L.Y. (2003), “Analytical study of wind-rain-induced cable vibration: SDOF model”, *J. Wind Eng. Ind. Aerodyn.*, **91**, 27-40.

Yamaguchi, H. (1990), “Analytical study on growth mechanism of rain-wind induced vibration of cables”, *J. Wind Eng. Ind. Aerodyn.*, **33**, 73-80.

GS